Magnetotransport in Dual-Gated Bilayer Graphene

XXXXXXXX*
Department of Physics and Astronomy, University of British Columbia
6224 Agricultural Road, Vancouver, British Columbia, Canada, V6T 1Z1
(Dated: November 13, 2010)

Bilayer graphene, two single-atom-thick sheets of carbon stacked upon each other, is a unique system in which the size of the band gap can be continuously tuned through the application of a perpendicular electric field. We propose to fabricate dual-gated bilayer graphene electronic devices in which this effect can be realized. We will then measure magnetoconductivity in such devices at temperatures below 4 K to probe weak localization, a quantum interference effect. By examining the effects of a variable band gap on weak localization, we hope to gain further physical insight into electronic transport in bilayer graphene.

PACS numbers:

I. MOTIVATION

Since its first isolation in 2004 [1], graphene, a single-atom-thick sheet of carbon arranged in a honeycomb lattice, has continued to fuel enormous amounts of research activity. While its very existence is remarkable, defying a long-standing prediction that two-dimensional crystals are thermodynamically unstable [2, 3], its electronic properties are even more fascinating and hold much promise for technological and scientific advancements alike. High charge carrier mobilities in graphene give it potential to replace silicon in transistor applications. Long coherence times make it a candidate material for future quantum computers. From a physics point of view, graphene's massless charge carriers travelling at an effective speed of light ($\sim 10^6$ m/s) [4] is an example of quantum electrodynamics witnessed outside the confines of large particle accelerators. Also, its honeycomb lattice is composed of two triangular sublattices (Figure 1(a)), and the electronic density can be on one sublattice or the other, or a superposition of both. This two-level sublattice degree of freedom is analogous to spin-$\frac{1}{2}$ and is appropriately called pseudospin. Unlike spin-$\frac{1}{2}$, it does not couple to an external magnetic field, but it results in exotic quantum hall behaviour in graphene [5, 6]. With the abundance of unique properties in graphene, this year's awarding of the Nobel Prize in Physics to its discoverers a mere six years after its discovery is clearly not unwarranted.

Unlike other semiconductors, graphene has no band gap and exhibits a sizable finite conductivity even at zero charge carrier density [5, 6]. While this is physically interesting, it is a severe hindrance to the realization of graphene transistors, which require a conducting (on) and an insulating (off) state. Much of this motivates the study of bilayer graphene (BLG), two single-atom-thick sheets of carbon stacked upon each other. Under normal conditions, BLG also lacks a band gap. However, it possesses a novel feature: when a perpendicular electric field is applied across the two sheets of the bilayer, a band gap is opened and its size can be continuously tuned [7–9]. This is easily achieved in a dual-gated BLG electronic device [8, 9]. Thus, this tuning of the band gap in bilayers offers a possible path towards fabricating graphene transistors.

In light of transistor applications, many experiments on bilayers have focused on opening larger band gaps and characterizing their size (e.g., Refs. 9-11). However, the physical properties of BLG with an electrostatically-opened band gap (called biased BLG) are equally as interesting. Biased BLG has been the subject of much theoretical investigations, with predictions ranging from hyperbolic energy dispersions [7] to ferromagnetic states [12] to unusual Landau level behaviour [13]. Many of these phenomena are best probed by magnetotransport measurements, i.e., electrical measurements of conductivity in the presence of a magnetic field, in dual-gated BLG devices. Presently, most magnetotransport measurements in dual-gated BLG have focused on the high field ($B > 1$ T) regime (e.g., Refs. 14, 15). To our knowledge, there has been no experimental work in the low-field ($B < 1$ T) regime. Thus, we propose to study low-field magnetotransport in dual-gated bilayer graphene.

Low-field magnetotransport measurements in 2D systems often involve studies of weak localization (WL), a quantum effect arising from the interference of electron waves. From examining WL, the inelastic dephasing rate can be extracted, and in graphene, additional elastic electron scattering rates can also be obtained [16, 17]. Together, these scattering rates and their dependencies on different parameters provide physical insight into electronic transport in graphene. For example, the linear temperature dependence of the dephasing rate τ_ϕ^{-1} is an indication that electron-electron interactions are the main mechanism for inelastic scattering [16, 17]. As another example, graphene is usually rippled, and the dependence of τ_ϕ^{-1} on a magnetic field applied in the average plane of the graphene flake allows for an estimate of ripple size [18]. In dual-gated BLG, we can exploit the tunable band gap as an extra parameter with which

*Electronic address: XXXX.com

to study WL. By analyzing how the different scattering rates change with the band gap size, we hope to gain a more complete understanding of electronic transport in BLG.

II. THEORY

We review the band structure of graphene and the origins of the tunable band gap in BLG. We then discuss weak localization theory both in a general setting and in the specific context of graphene.

A. Band Structure of Graphene

Graphene's energy bands are derived from a tight-binding Hamiltonian, and near certain points in **k**-space called the Dirac points, the bands can be expanded in the low energy limit to yield to following energy dispersion relation:

$$E_{\pm} \approx v_F \left|\mathbf{k}\right|, \tag{1}$$

where v_F is the Fermi velocity and **k** is the momentum measured with respect to the Dirac point [19]. This linear energy dispersion gives rise to massless charge carriers, and indeed Eq. 1 is reminiscent of the photon equation $E = pc$. Also, as seen in Figure 1(b), the valence and conduction bands intersect at $E = 0$, so there is no band gap.

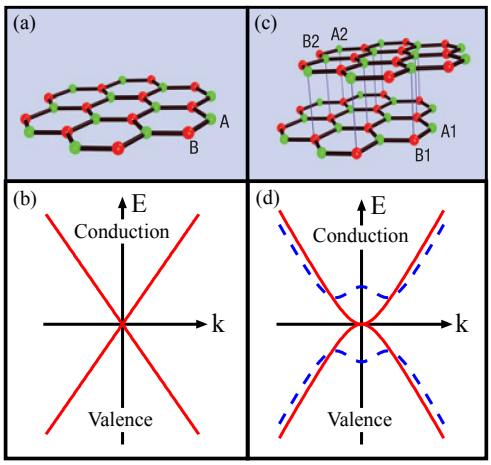

FIG. 1: (a) (from Ref. 8) The honeycomb lattice of monolayer graphene can be decomposed into two interwoven triangular sublattices, labelled by green and red. (b) Linear energy dispersion of monolayer graphene. The valence and conduction bands intersect at the origin, resulting in zero band gap. (c) (from Ref. 8) BLG has a total of four sublattices, but only two (labelled A1 and B2) are relevant in low energy considerations. (d) The gapless quadratic energy dispersion (red) of bilayer graphene becomes gapped and hyperbolic (blue) upon application of a perpendicular electric field.

Physically, this zero band gap originates from the fact that graphene's hexagonal lattice can be decomposed into two triangular sublattices (see Figure 1(a)), and the two sublattices are degenerate. To open a band gap, we could introduce an energy difference betweeen the sublattices, but since they are interwoven and lie in the same plane, this is difficult to implement experimentally.

Bilayer graphene consists of a total of four triangular sublattices, but it happens that only two of these sublattices, labelled A1 and B2 in Figure 1(c), are relevant in the low energy limit [8]. Its energy dispersion is quadratic (Figure 1(d)) and results in massive charge carriers, but again is not gapped. This also arises from the degeneracy of the sublattices A1 and B2, except in this case, the two sublattices lie on different planes. Thus, the application of a perpendicular electric field will induce a potential difference between A1 and B2 and open a gap in the energy dispersion (Fig. 1(d)).

B. Weak Localization [20]

In the path integral formulation of quantum mechanics, the probability associated with a particle moving from points A to B is given by the magnitude-squared of some complex amplitude $\Psi_{A\to B}$. This amplitude is computed by summing over the individual contributions $\psi_i = A_i e^{i\phi_i}$ from every possible trajectory between A and B (Figure 2(a)):

$$\Psi_{A\to B} = \sum_{all\ paths} A_i e^{i\phi_i} \tag{2}$$

This probability of propagation can be associated with conductivity in 2D systems when electron transport is diffusive. At low temperatures, inelastic scattering is reduced, allowing electrons to maintain phase coherence over long distances; i.e., the relative phases $\Delta\phi_i$ between the different possible trajectories in Fig. 2(a) are constant over some characteristic length. This allows for constructive and destructive interference when the individual contributions $A_i e^{i\phi_i}$ are summed. Normally, the phases between the possible trajectories are uncorrelated and average out in the sum in Eq. 2, and the resulting conductivity is that of the classical Drude conductivity, with no input of quantum mechanics.

The situation is different, however, in the case of a closed loop trajectory. When time-reversal symmetry is present, the closed loop path and its counterpropagating partner accumulate the same phase, so the contributions from these two trajectories interfere constructively (Figure 2(b)). Thus, the probability for closed loop paths, in which electrons remain "localized," is enhanced, resulting in an overall decrease in conductivity. This is weak localization - a negative correction term to the classical Drude conductivity originating from quantum interference considerations.

Physically, only the total conductivity, $g = g_{Drude} + \Delta g_{WL}$, where $\Delta g_{WL} < 0$, is readily measured. To probe

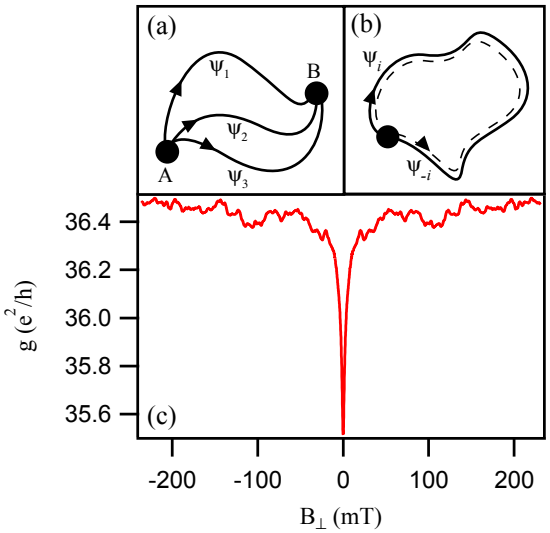

FIG. 2: (a) Feynman path integral formalism. The complex amplitude associated with the probability of a particle moving from points A to B is given by the sum of individual contributions ψ_i from all possible trajectories between A and B. (b) The closed-loop trajectory ψ_i interferes constructively with its time-reversed partner ψ_{-i}, resulting in weak localization. (c) Suppression of weak localization in a magnetoconductivity $g(B_\perp)$ trace. As the magnitude of $B_\perp$ increases, g is restored.

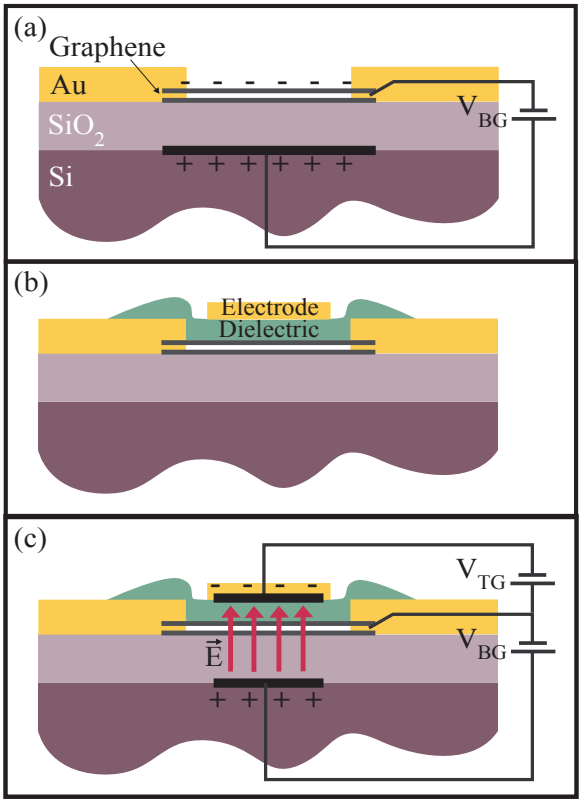

FIG. 3: (a) The charge carrier density of a graphene flake can be capacitatively tuned by applying a back gate voltage. (b) A full dual-gated BLG device. (c) Alternatively, we can view the bottom gate as one plate of a capacitor and the top gate as another. By applying V_{BG} and V_{TG} in opposite polarities, we can establish an electric field across the bilayer flake.

WL, we need to examine magnetoconductivity, the dependence of conductivity on magnetic field. A small perpendicular magnetic field $B_\perp$ has the effect of breaking the symmetry between a closed loop trajectory and its time-reversed partner. The two paths now accumulate different phases and constructive interference is lost, restoring the total conductivity. The resulting $g(B_\perp)$ curve is shown in Figure 2(c): g has a minimum at zero field, and rises monotonically with increasing field.

In most 2D systems, the functional form of the magnetoconductivity $g(B_\perp)$ depends only on the inelastic dephasing rate, τ_ϕ^{-1}. In graphene however, due to the pseudospin degree of freedom, WL is also affected by the elastic intervalley scattering rate τ_i^{-1} and the elastic intravalley scattering rate τ_*^{-1}. Thus, the situation is much more complicated in graphene, and the precise balance of these three scattering rates determines whether WL is suppressed or enhanced, or whether weak antilocalization (WAL) is observed instead [21].

III. DEVICE FABRICATION AND DUAL-GATE GEOMETRY

Flakes of monolayer and bilayer graphene are produced by mechanically-exfoliating graphite pieces with Scotch tape and transfering the graphitic residue from the tape to Si wafers. The Si substrate has a $\sim$ 300 nm-thick overlayer of SiO_2, which allows a thin-film interference effect to take place. This causes atomically-thin and transparent graphene flakes to be visible under an optical microscope, and even their number of layers to be resolved. Next, the flakes are contacted with Au electrodes through electron-beam lithography with scanning electron microscopy in order to fabricate micron-sized graphene electronic devices.

The Si/SiO_2 substrate also serves as a back gate. If we visualize the graphene flake as one plate of a capacitor, the Si as another and the SiO_2 in between as an insulating dielectric layer, then the charge carrier density of the flake can be capacitatively tuned by applying a back gate voltage (Figure 3(a)). Similarly, we can construct a top gate by depositing some insulating material on top of the flake, followed by another metal electrode (Figure 3(b)). Now we have two gates, and by applying voltages of the same polarity to both gates, an increased charge carrier density can be induced.

Alternatively, we can view the bottom and top gates as a single capacitor with the graphene flake as something sandwiched in between (Figure 3(c)). Then if we apply voltages of opposite polarities to the bottom and top

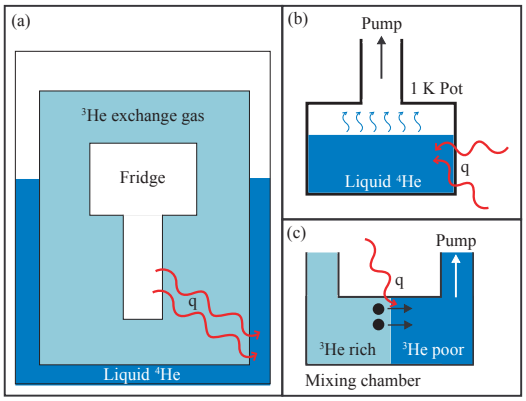

FIG. 4: Three main cooling mechanisms of the dilution fridge: (a) Thermal contact between the fridge and a reservoir of liquid ^{4}He through an exchange gas brings the fridge temperature down to 4 K. (b) Pumping on liquid ^{4}He further lowers the temperature via evaporative cooling down to 1 K. (c) In the mixing chamber, a ^{3}He/^{4}He mixture separates into a ^{3}He-rich phase and a ^{4}He-poor phase. The crossing of a ^{3}He atom from the rich to poor phase is endothermic and provides further cooling down to 20 mK.

gates, a perpendicular electric field across the graphene is generated. This is how a tunable band gap can be achieved in a dual-gated BLG device.

Most top gate fabrication procedures require two steps: Deposition of an insulating layer, then fabrication of a metal electrode over the insulating layer. However, Miyazaki *et al.* discovered that when they evaporated Al directly onto graphene then exposed the entire device to air, an insulating oxide layer spontaneously formed between the graphene-Al interface[22]. This one-step procedure produces highly efficient top gates and we propose to fabricate most of our devices in this manner.

IV. MEASUREMENT AND APPARATUS

Electrical measurements of micron-sized devices involve currents on the scale of nanoamps. To extract such tiny signals embedded in a noisy environment, we use SR830 lock-in amplifiers and Ithaco current preamplifiers.

Many quantum mechanical phenomena, including weak localization, are often enhanced at temperatures below 4 K. The Quantum Devices Lab has an Oxford dilution fridge with a base temperature 20 mK. The refigeration process involves three main steps. First, the fridge is brought in thermal contact with a bath of liquid ^{4}He, which has a boiling point of 4 K (Figure 4(a)). Next, a pump is applied to a certain portion of that liquid ^{4}He contained in a 1 K pot, and the evaporation of ^{4}He cools the pot down to 1 K (Figure 4(b)). Finally, the 1 K pot is used to cool a mixture of ^{3}He/^{4}He until a phase separation between a ^{3}He-rich phase and ^{3}He-poor phase is attained. The crossing of a ^{3}He atom from the rich phase to the poor phase is endothermic and provides cooling down to 20 mK.

The dilution fridge also has a small superconducting magnet. Magnetic fields up to $\sim$ 200 mT can be applied.

V. PLANNED SCHEDULE

Task	Date
Fabrication of dual-gated BLG devices in AMPEL cleanroom	June-July
Measurement of device in dilution fridge	Aug
Data analysis	Sept-Oct
Further device fabrication and measurement	Nov-Dec
Further data analysis and progress report	Jan-Feb
Thesis write-up	Mar

VI. ACKNOWLEDGEMENTS

I would like to thank my supervisor, Dr. YYYY for giving me an opportunity to work in the Quantum Devices Lab and for all his guidance. I would also like to acknowledge Dr.XXX and Y for their involvments in this project, and also thank all the other awesome students at the lab. Special thanks to Y for some LaTex and Adobe Illustrator tips without which I probably would have spent many more hours in frustration.

[1] K. S. Novoselov *et al.*, Science **306**, 666 (2004).
[2] R. E. Peierls, Ann. I. H. Poincare **5**, 177222 (1935).
[3] L. D. Landau, Phys. Z. Sowjetunion **11**, 26-35 (1937).
[4] A. K. Geim, Nature Mat. **6**, 183-191 (2007).
[5] K. S. Novoselov *et al.*, Nature **438**, 197-200 (2005).
[6] Y. Zhang *et al.*, Nature **438**, 201-204 (2005).
[7] E. McCann, Phys. Rev. B **74**, 161403 (2006).
[8] J. B. Oostinga, *et al.*., Nature Mat. **7**, 151-157 (2007).
[9] Y. Zhang *et al.*, Nature **459**, 820-823 (2009).
[10] K. F. Mak *et al.*, Phys. Rev. Lett. **102**, 256405 (2009).
[11] B. N. Szafranek *et al.*, Appl. Phys. Lett. **96**, 112103 (2010).
[12] E. V. Castro *et al.*, Phys. Rev. Lett. **100**, 186803 (2008).
[13] C. Toke, and V. I. Fal'ko, arXiv:1008.3259v1.
[14] E. A. Henriksen and J. P. Eisenstein, Phys. Rev. B. **82**, 041412 (2010).

[15] R. T. Weitz *et al.*, Science **330**, 6005 (2010).
[16] R. V. Gorbachev *et al.*, Phys. Rev. Lett. **98**, 176805 (2007).
[17] F. V. Tikhonenko *et al.*, Phys. Rev. Lett. **100**, 056802 (2008).
[18] M. B. Lundeberg and J. A. Folk, Phys. Rev. Lett. **105**, 146804 (2010).
[19] A. H. Castro Neto *et al.*, Rev. Mod. Phys. **81**, 109-162 (2009).
[20] For a review of weak localization theory, we refer the reader to C. W. J. Beenakker and H. van Houten, Solid State Physics **44**, 1 (1991).
[21] F. V. Tikhonenko *et al.*, Phys. Rev. Lett. **103**, 226801 (2009).
[22] H. Miyazaki *et al.*, Semiconductor Science and Tech. **25** 034008 (2010).